Environmental Research 237 (2023) 117101

Contents lists available at ScienceDirect

Environmental Research

journal homepage: www.elsevier.com/locate/envres

Assessment of source-oriented health risk associated with the oral ingestion of heavy metals in dust within an iron/steel smelting-affected area of the North China Plain

Mingya Wang [a], Xiaohang Xu [b,c], Qiao Han [b,*], Xihuang Lin [d], Haijun Yuan [b], Mingshi Wang [a], Fengcheng Jiang [a], Wenju Wang [a]

[a] College of Resource and Environment, Henan Polytechnic University, 454003, Jiaozuo, China
[b] State Key Laboratory of Environmental Geochemistry, Institute of Geochemistry, Chinese Academy of Sciences, 550081, Guiyang, China
[c] Key Laboratory of Karst Georesources and Environment, Ministry of Education, Colleage of Resources and Environmental Engineering, Guizhou University, 550025, Guiyang, China
[d] Analysis and Test Center, Third Institute of Oceanography, Ministry of Natural Resources, 361005, Xiamen, China

ARTICLE INFO

Keywords:
Heavy metals
Windowsill dust
Iron/steel smelting
North China plain
In vitro digestion tests (PBET)
Source-specific exposure risks

ABSTRACT

Heavy metals (HMs) from iron/steel smelting activities pose notable risks to human health, especially to those living around industrial facilities of North China Plain, the base of China's steel production. In this study, 78 outdoor windowsill dust samples were collected around a large-scale iron/steel smelter with more than 65 years of production history in the western North China Plain. Nine HMs were analysed to comprehensively assess the health risks by integrating Monte Carlo simulation, oral bioaccessibility, and source apportionment. Results showed serious pollution with Cd, Pb, and Zn based on their geo-accumulation index values and concentrations. Four potential sources including industrial sources (49.85%), traffic sources (21.78%), natural sources (20.58%), and coal combustion (7.79%) were quantitatively identified by multivariate statistical analysis. The oral bioaccessibilities of HMs determined by the physiologically based extraction test ranged from 0.02% to 65.16%. Zn, Mn, Cd, and Pb had higher bioaccessibilities than other HMs. After incorporating oral bioavailability adjustments, noncarcinogenic and carcinogenic risks were significantly reduced, especially for adults. The mean hazard index (*HI*) for children and adults was below the safety threshold (1.0), whereas the mean of the total carcinogenic risk (*TCR*) based on HM bioaccessibilities in the gastric phase remained above the acceptable level (1.0E-06) (children: 5.20E-06; adults: 1.16E-06). Traffic sources warranted increased concern as it substantially increased *TCR*. Cd was identified as the priority pollution in iron/steel smelting areas. Assessing source-oriented health risks associated with oral ingestion exposure can guide the management and control of HM contamination within iron/steel smelting-affected areas.

1. Introduction

The iron/steel industry is one of the primary pillar industries of developing countries with rapid economic growth (Dong et al., 2013). However, numerous toxic chemicals are produced during smelting and they enter the environment along with flue gas, waste rock, smelting slag, and other substances (Ahamad et al., 2021; Soltani et al., 2021; Han et al., 2021a; Zhang et al., 2022). Among them, heavy metals (HMs) such as Hg, Cd, and As are important pollutants of concern owing to their toxicity and adverse impact on human health and biota (Luo et al., 2011; Kastury et al., 2018; Han et al., 2020). When exposed to such affected environments, the unintentional oral ingestion of contaminated soil and dust is a potentially important route for residents to be exposed to HMs (Zahran et al., 2013; Wang et al., 2023; Ma et al., 2021). Particularly, HMs in dust are more easily resuspended and spread locally and globally than in soils, posing a threat to human health (Zgobicki et al., 2019). Thus, investigating the contaminant levels of dust near iron/steel smelting-affected areas and understanding the health exposure risk of HMs for local residents are necessary.

Many studies on health-risk assessment including noncarcinogenic and carcinogenic risks primarily rely on human health-risk assessment (HHRA) models with specific fixed exposure factors and average HM

* Corresponding author.
E-mail address: hanqiao@mail.gyig.ac.cn (Q. Han).

https://doi.org/10.1016/j.envres.2023.117101
Received 10 May 2023; Received in revised form 8 August 2023; Accepted 6 September 2023
Available online 7 September 2023

concentrations (Khan et al., 2016; Yadav et al., 2019; Han et al., 2021a). However, ignoring the variations in exposure parameters across populations and the uncertainty of HM concentrations may lead to inaccurate assessment results (Ganyaglo et al., 2019). Fortunately, Monte Carlo simulation (MCS), an effective probabilistic analysis measure to compensate for this deficiency, can provide a reliable and informative result by calculating the proportion of surpassing and not surpassing the safety threshold (Sun et al., 2022). Humans can be exposed to HM pollution via three pathways (oral ingestion, inhalation, and dermal contact). However, many previous studies have found that oral ingestion contributes most to the overall health risks of HMs (Gu and Gao, 2018; Ganyaglo et al., 2019; Jin et al., 2019) especially children due to their repeated hand/finger sucking (Han et al., 2020). Therefore, only the health risks of oral ingestion of HMs in dust were assessed in the present study.

Remarkably, HMs originating from various pollution sources show significant variations in content, toxicity coefficients, bioavailability, and health hazards (Ma et al., 2021). Determining the crucial pollution sources and key pollution factors is a prerequisite for reducing the emissions of new HMs and the associated health risks. However, the traditional concentration-based HHRA model overestimates the health exposure risks and inaccurately identifies high-risk sources and priority HMs (Liu et al., 2019; Han et al., 2020; Ning et al., 2021), leading to ineffective management of HM contamination. Therefore, incorporating source apportionment into the HHRA model is receiving increased attention (Liu et al., 2018, 2021a; Ma et al., 2021; Yan et al., 2022). Compared with other receptor models, the positive matrix factorisation (PMF) model has been confirmed to obtain each contamination source's category and contribution rate through the least square method (Paatero and Tapper, 1994; Huang et al., 2021; Zhao et al., 2022). In the current work, MCS and the PMF model were combined in the HHRA model to identify key sources of pollution and quantify the human health risks accurately.

Given that only a fraction (≤100%) of HMs can be absorbed by the gastrointestinal system after human ingestion, the traditional HHRA model based on total HM concentrations may exaggerate the health hazard of contamination sources (Aurelie et al., 2011; Kastury et al., 2018; Han et al., 2021b). Thus, incorporating bioaccessibility into the HHRA model is necessary. Bioaccessibility is defined as the proportion of HMs that can be dissolved and adsorbed by tissue fluids of the lungs, intestines, and stomach (Ruby et al., 1996, 1999). Several *in vivo* and *in vitro* digestion tests have been successfully designed to determine HM bioaccessibilities (Mehta et al., 2020; Han et al., 2023). Generally, the results of testst on *in vivo* animal models are more convincing and accurate. However, these tests are time consuming and costly and involve ethical controversy, limiting the application of this method (Zia et al., 2011). To hurdle this limitation, *in vitro* digestion models are developed as alternatives to simulate the animal organism environment *in vitro* and are extensively applied to measure HM bioaccessibilities, specifically the physiologically based extraction test (PBET) (Gu and Gao, 2018; Delbeke et al., 2020; Ma et al., 2022). Previous studies have shown that PBET exerts a better fitting effect with the results of *in vivo* animal experiments than other *in vitro* digestion methods (Juhasz et al., 2010; Pan et al., 2016; Wei et al., 2021). Nevertheless, to our knowledge, few studies have expanded on integrating bioaccessibility and MCS in source-oriented health-risk assessment. Hence, systematically combining oral bioaccessibility, MCS, source apportionment, and the HHRA model is necessary to evaluate the health hazard of HMs in dust within iron/steel smelting-affected areas.

The North China Plain, also known as China's iron/steel production base, has many iron/steel smelting-dependent industrial facilities. According to the World Steel Association (2020) and Chinese Statistical Yearbook (2020), the total production of crude steel in the North China Plain was approximately 459.42 million tons in 2019, accounting for nearly 25% of the world's steel production (WSA, 2020; NBSC, 2020). Intensive iron/steel smelting activities and related industrial activities such as transportation, coal burning, and coking have led to the severe contamination of the soil and atmosphere with HMs in the region (Han et al., 2021a, 2021b; Liu et al., 2021b; Wang et al., 2023). However, no related studies have been conducted on the bioaccessibilities, exposure risks, and source contributions of HMs in dust near iron/steel smelters in the North China Plain. This lack of knowledge hinders the implementation of pollution control and risk management in HMs.

To fill this knowledge gap, we selected a large iron/steel smelting-affected area in the western North China Plain as the research area in the present work. The primary objectives of this study were as follows: (i) to determine the concentrations and contamination characteristics of HMs in outdoor windowsill dust within the iron/steel smelting-affected area; (ii) to identify pollution sources of HMs through multivariate statistical analysis, including geostatistical analysis, Pearson correlation analysis, clustering analysis, and the PMF model; and (iii) to quantify human health exposure risks and identify the critical pollution factors by coupling PBET, MCS, the PMF model, and the HHRA model.

2. Materials and methods

2.1. Study area and sampling

This study area is located in Anyang, Henan Province in the western North China Plain (Fig. 1). It has been affected by long-term (>65 years) iron/steel smelting activities. The research region has a warm temperate continental monsoon climate with an average annual temperature, precipitation, and wind speed of 14.2 °C, 600 mm, and 2.2 m/s, respectively (Han et al., 2021a). The prevailing wind direction in winter and summer is northeast and southwest, respectively. Since 1993, Anyang has been involved in HM industries, including ferrous-metal smelting, steel rolling, coking, and cement production. In 2019, Anyang produced approximately 15.09 million tons of steel, among which the iron/steel smelter investigated in this study accounted for 69.85% (10.54 million tons), ranking 41st in the world (WSA, 2021).

A total of 78 outdoor windowsill dust samples were collected from 23 communities surrounding the iron/steel smelter in November 2019. Before and during sampling, no rainfall and gale activity occurred for 7 consecutive days. The number of dust samples collected in each community was determined according to their area and population. Sampling sites were located within the community, about 50–100 m from the main traffic roads. No obvious pollutants and pollution sources were found near the sampling sites. The distance between adjacent sampling points exceeded 50 m in each community. Dust samples were collected using plastic brushes and dustpans from the lowest-story outdoor windowsills of the residential building, which were 10–30 cm wide and approximately 1.0–1.5 m above the ground. Each sample was collected from 6 to 10 windowsills within 100 m^2 to obtain sufficient dust. After each sampling, sampling tools were cleaned with deionised water to prevent cross-contamination between samples. All collected composite dust samples were naturally dried indoors, and then extraneous materials (such as dead leaves, hair, insect shells and gravel) were removed from samples with plastic clips. Finally, dust samples were passed through a 200-mesh nylon sieve (<75 μm) for further chemical analysis.

2.2. PBET

PBET analysis was performed based on previously described research with minor modifications to determine the bioaccessibilities of HMs (Ruby et al., 1996; Han et al., 2020). In the gastric phase (PBETG), 2.0 g of the sieved dust sample was extracted using 200.0 mL of simulated gastric solution (1.25 g of pepsin, 0.5 g of citric acid, 0.5 g of malic acid, 0.42 mL of lactic acid, 0.5 mL of glacial acetic acid, and 8.775 g of NaCl dissolved in 1000 mL of ultrapure water; pH adjusted to 1.5 with concentrated HCl) in a 500 mL cone bottle. The mixture was sealed, warmed to 37 °C in a water bath, and shaken at 100 $r \cdot min^{-1}$ for 1.0 h. Then, 30.0 mL of the suspension was collected and filtered through a

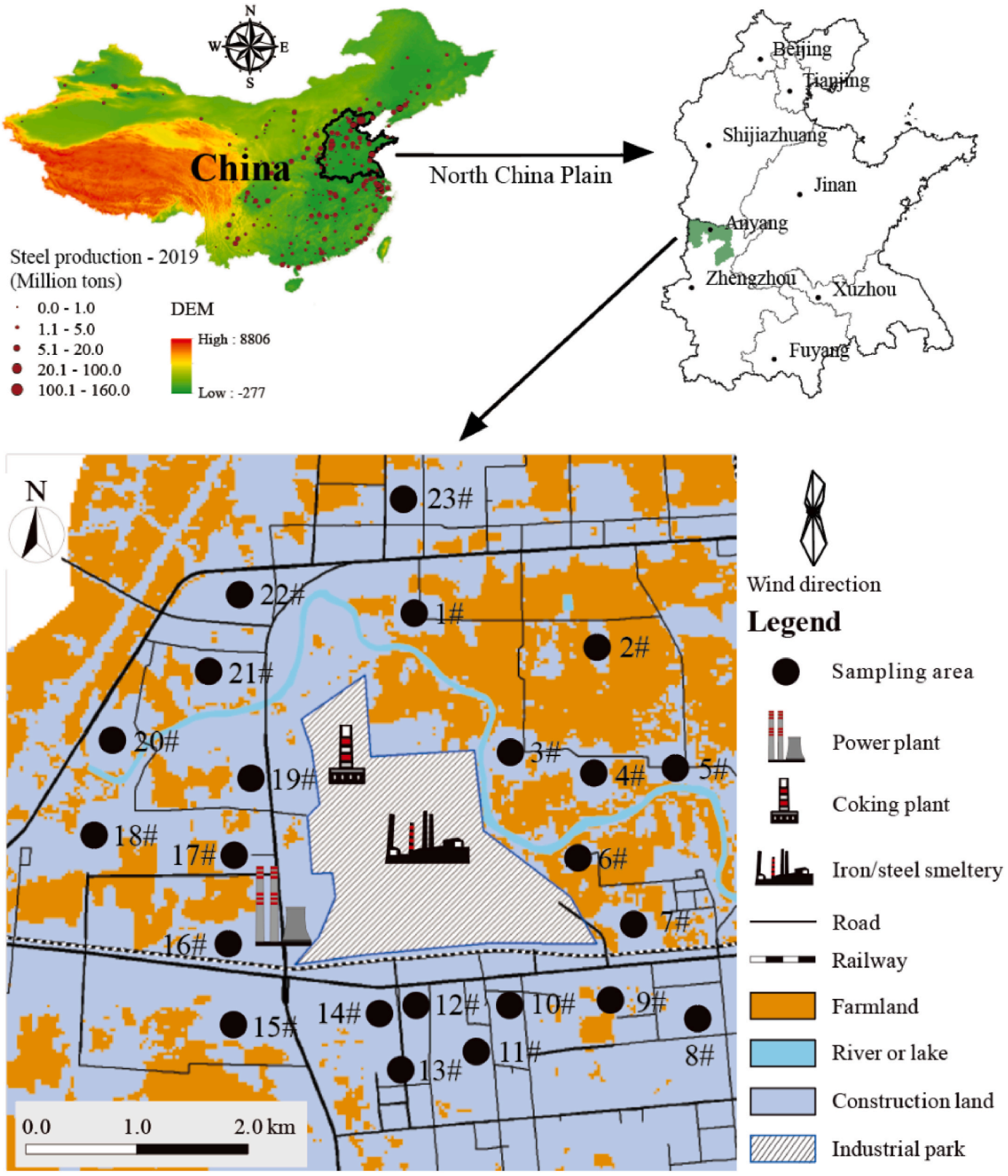

Fig. 1. Study region and sampling area.

0.45 μm nitrocellulose membrane. In the intestinal phase (PBETI), the rest solution was adjusted to a pH of 8.0 with concentrated $NaHCO_3$ solution, and 0.4 g of bile salts and 1.2 g of trypsin were added into the cone tube. Then, the sample solution was sealed and shaken for 4.0 h at 37 °C. Finally, 30.0 mL of suspension was collected and filtered through a 0.45 μm nitrocellulose membrane. ICP−MS was used to determine the concentration of HMs in suspension ordered in PBET. The bio-accessibilities of HMs (*BAF*, %) can be calculated by dividing the bio-accessible HM concentrations by the total HM concentrations in the sample (Han et al., 2020), as shown in Equation (1).

$$BAF = ((C_i \times V_i) / (C_s \times m_s)) \times 100 \quad (1)$$

where C_i is the soluble concentration of HMs extracted by PBET (mg/L), V_i is the reaction liquid volume (L), C_s is the total HM concentrations (mg/kg), and m_s is the mass of the sample (kg).

2.3. Geochemical analysis

For the HM concentration assays, 0.10 g of the sieved dust sample was digested using a concentrated acid mixture (4.0 mL of HNO_3, 1.5 mL of H_2O_2 and 1.5 mL of HF) in a Teflon microwave tube. Digestion primarily included three steps. First, the digestion tubes were heated to 120 °C and held for 10 min, continued to be heated to 260 °C, and held for 45 min. When cooled to 70 °C, the digestion tubes were transferred into an acid-removing instrument at 120 °C for 150 min. Finally, the remaining solution in the digestion tube was transferred into a volumetric flask for constant volume using 5% HNO_3 solution and then filtered through a 0.45 μm nitrocellulose membrane. The total concentration of HMs was measured by ICP–OES. Glassware and other experimental instruments were cleaned with 10% HNO_3 solution to avoid background contamination. Method blanks (20%), parallels (10%), and GBW07401 (National Institute of Standard Materials, China) were determined to verify the accuracy of the experiment. The relative deviations between the measured and standard values for Cd, Co, Cr, Cu, Mn, Ni, Pb, V, Zn, and As were 10.42%, 7.03%, 6.03%, 4.11%, 8.06%, 6.25%, 3.64%, 4.69%, 7.13%, and 7.30%, respectively.

2.4. Contamination assessment

The geo-accumulation index (I_{geo}) and improved Nemerow index (*INI*) introduced by Liu et al. (2020) were applied to evaluate the overall and individual contamination levels of HMs. I_{geo} and *INI* were calculated using Equations (2) and (3):

$$I_{geo} = \log[C_s / (1.5 \times C_b)] \quad (2)$$

$$INI = \sqrt{\left(I_{geo_{\max}}^2 + I_{geo_{\text{avg}}}^2\right) / 2} \quad (3)$$

where C_s and C_b are the HM contents in the sample and regional background, respectively; and $I_{geo\ \max}$ and $I_{geo\ \text{avg}}$ are the maximum and mean I_{geo}, respectively. The contamination degrees of I_{geo} and *INI* are shown in Table S1.

2.5. HHRA model

The HHRA model was adopted to assess the health hazards posed by HMs to adults and children (USEPA, 1989, 2009, 2011). Results showed that Cd, Co, Cr, Cu, Mn, Ni, Pb, V, and Zn presented chronic noncarcinogenic health risks to humans, and some of them (Cd, Cr, and Pb) also exerted carcinogenic health risks. For the exposure-assessment model, the daily intake (*ADD*, mg/kg·day) based on the total concentration or oral bioaccessible concentration of HMs was first calculated by Equations (4) and (5):

$$ADD_{\text{ing}-total\ \text{concentration}} = \left(c \times R_{ing} \times EF \times ED \times 10^{-6}\right) / \left(BW \times AT\right) \quad (4)$$

$$ADD_{\text{ing}-\text{oral bioaccessibility}} = ADD_{\text{ing}-total\ \text{concentration}} \times BAF \quad (5)$$

The overall carcinogenic risk (hazard index, *HI*) and total noncarcinogenic risks (*TCR*) of oral ingestion for multiple HMs were assessed according to the hazard quotient (*HQ*) and carcinogenic (*CR*) of each HM, respectively, as estimated by Equations (6) and (7).

$$HI = \sum HQ = \sum ADD / RfD \quad (6)$$

$$TCR = \sum CR = \sum ADD \times SF \quad (7)$$

For noncarcinogenic risks, *HQ* or *HI* > 1.0 means possible adverse health effects, and conversely, noncarcinogenic risks (USEPA, 2011). For carcinogenic risks, *CR* or *TCR* > 1.0E-04 indicated significant carcinogenic risks for humans; if *CR* or *TCR* was between 1.0E-6 and 1.0E-4, the carcinogenic risks were acceptable. *CR* or *TCR* lower than 1E-06 indicated negligible carcinogenic risks (USEPA, 1989). The meaning and values of exposure factors in the above equations are described in Tables S2 and **S3**. Meanwhile, MCS simulations were conducted with 100 000 iterations at random (Han et al., 2022).

2.6. Source apportionment

The PMF model is a mathematical technique for quantitatively analysing the allocation of various contamination sources according to sample compositions or fingerprints (Paatero and Tapper, 1994; Song et al., 2021). The PMF model was calculated according to Equation (8):

$$x_{ij} = \sum_{k=1}^{p} g_{ik} f_{kj} + e_{ij} \quad (8)$$

where x_{ij} is the HM concentration; i and j are the sample number and chemical varieties, respectively; p is the source number; g_{ik} is the source contributions to samples; f_{kj} is the proportion of sources in HMs; and e_{ij} is the residual matrix. The PMF optimal result was determined by minimising the 'objective function' Q, as calculated by Equations 9–11.

$$Q = \sum_{i=1}^{n} \sum_{j=1}^{m} \left(e_{ij} / u_{ij}\right)^2 \quad (9)$$

$$\text{For } x_{ij} \le MDL,\ u_{ij} = \frac{5}{6} \times MDL \quad (10)$$

$$\text{For } x_{ij} > MDL,\ u_{ij} = \sqrt{\left(\sigma \times x_{ij}\right)^2 + (0.5 \times MDL)^2} \quad (11)$$

where u_{ij} is the iHM uncertainty, *MDL* is the detection limit of elements, and σ is the error fraction.

2.7. Data analysis

Statistical calculations were conducted with Microsoft EXCEL 2021 and IBM SPSS 23.0. Origin 2021 was used to plot the figures. The locations of the sampling region and the spatial characteristics of HM concentrations were constructed using ArcGIS 10.2. The uncertainty analyses of MCS were calculated using Oracle Crystal Ball (vs.11.1.2, USA) software and Origin 2021.

3. Results and discussion

3.1. Concentrations and pollution characteristics of HMs

Descriptive features for HMs in outdoor windowsill dust collected from the iron/steel smelting-affected area are displayed in Fig. 2. The average concentrations (mg/kg) of HMs were as follows: Mn (1475.19) > Zn (672.56) > Pb (228.99) > V (191.94) > Cr (143.35) > Cu (86.89) > Ni (28.10) > Co (15.77) > Cd (5.30). Compared with the relevant arithmetic average background soil values (CNEMC, 1990), the mean concentrations of Cd, Pb, and Zn were significantly elevated, except for Co, Cr, Cu, Mn, and V, which were slightly higher (Fig. S1a). This finding preliminarily indicated that Cd, Pb, and Zn contamination occurred at some sampling sites. Particularly, the mean concentration of Cd exceeded the background value by 75.71 times, which was much higher than those of the other HMs. The HM concentrations were compared with national soil quality standards (MEE, 2018). Only Cr and V had average concentrations higher than the relevant soil risk control standards (Fig. S1b). The maximum concentrations of Cr, Pb, and V were 9.18, 1.30, and 2.29 times the risk control standards of 30, 400, and 165

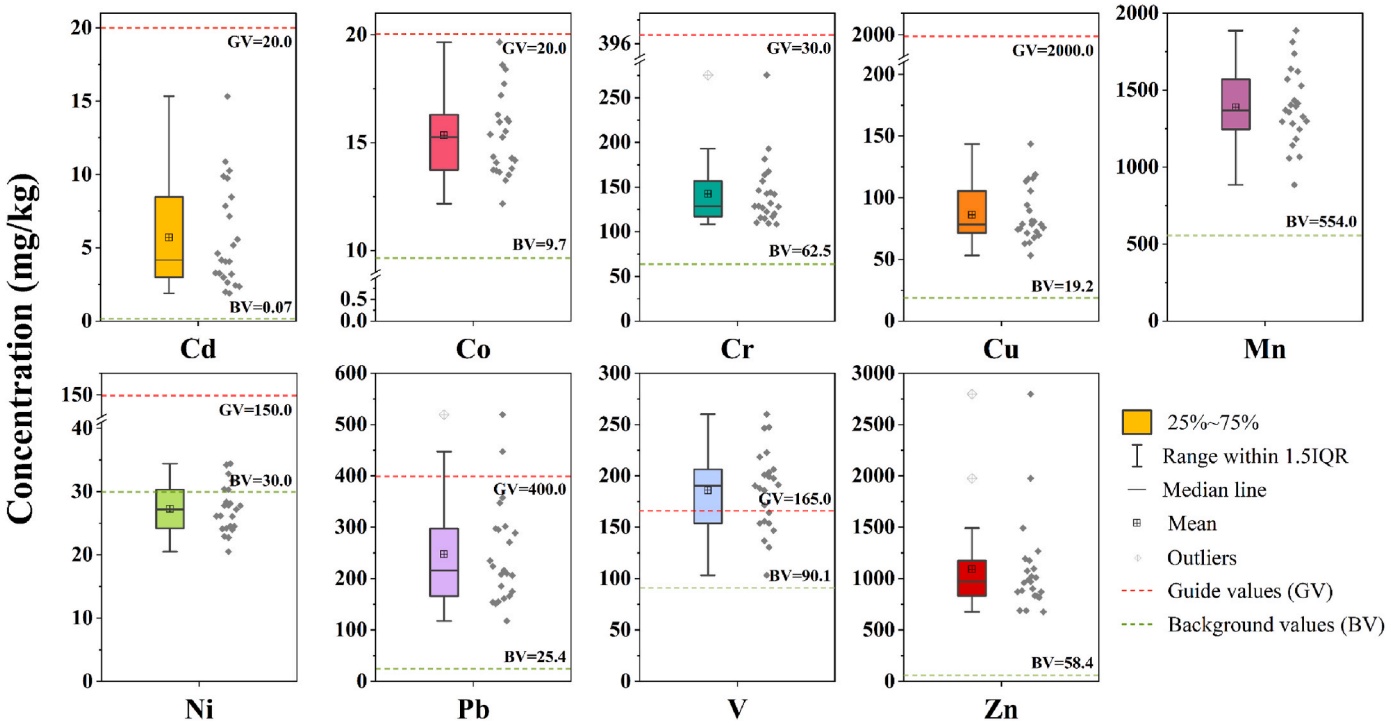

Fig. 2. Concentrations, control values (MEE, 2018), and background values (CNEMC, 1990) of HMs in windowsill dust.

mg/kg, respectively.

I_{geo} class distribution revealed that the contamination levels of HMs in dust were as follows: Cd > Pb > Zn > Cu > Mn > V > Cr > Ni > Co (Fig. S2a). Cd was the most serious, with I_{geo} values ranging within 4–8, and 91.30% of Cd I_{geo} exceeding 5, which was classified as extreme pollution. In all samples, 82.61%, 52.17%, and 65.22% of the I_{geo} values of Cu, Pb, and Zn, respectively, exceeded 2, indicating moderate to heavy pollution. The mean I_{geo} values of Cr, Mn, and V and I_{geo} in most sampling sites were between 0 and 1, exhibiting nonpollution to moderate pollution. Ni and Co were unpolluted (I_{geo} value < 0). *INI* values ranged from 3.56 to 5.79, with an average of 4.54, implying that the study area was heavily to extremely polluted by HMs in dust. About 21.74% of *INI* values were between 3 and 4, suggesting that these samples were heavily polluted, whereas 30.48% showed values above 5, corresponding with extreme pollution (Fig. S2b). This finding indicated that human activities greatly influenced HMs in dust, which was further

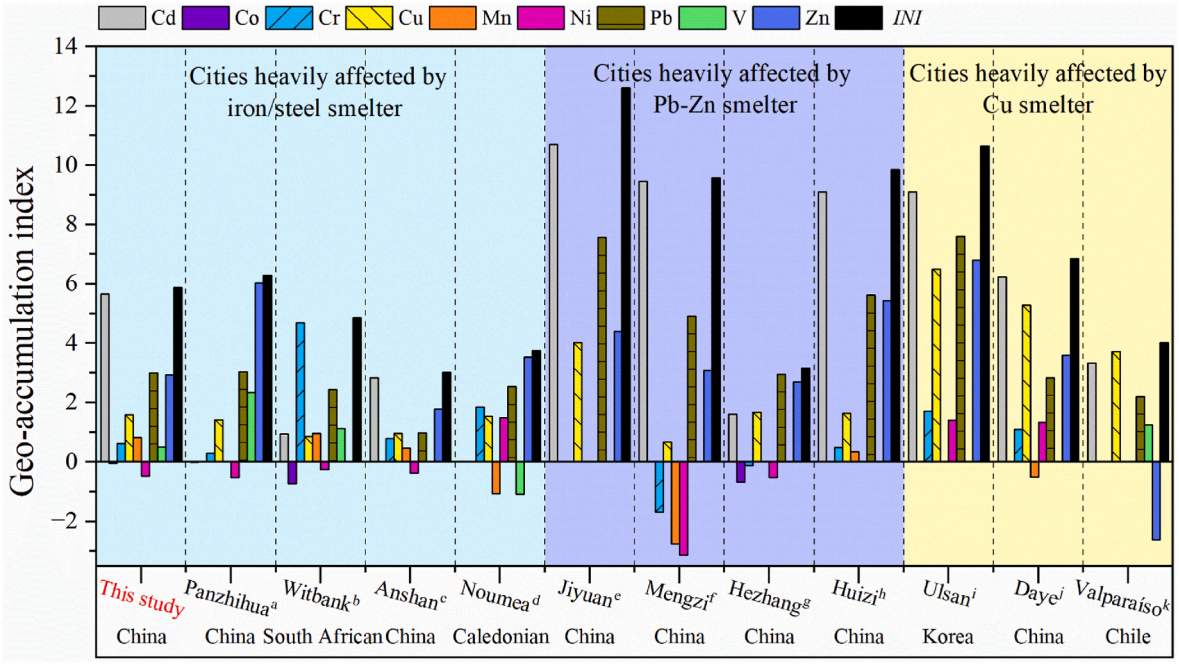

Fig. 3. Geo-accumulation indices of HMs in dust from different types of smelting-affected areas around the world ([a] Long et al., 2021; [b] Zibret et al., 2013; [c] Xiao et al., 2020; [d] Fry et al., 2021; [e] Xing et al., 2022; [f] Feng et al., 2020; [g] Wu et al., 2017; [h]Cao et al., 2020; [i] Jeong et al., 2021; [j] Wang et al., 2021; [k] Berasaluce et al., 2019).

confirmed by subsequent discussion. To better describe the effects of smelting activities on HM contamination in dust, Fig. 3 compares the I_{geo} values of HMs from cities heavily affected by iron/steel smelters and other smelters worldwide. Detailed information regarding the characteristics of the samples from other cities can be found in Tables S4 and S5.

Compared with the other four cities affected by the iron and steel smelting industries, the I_{geo} values of Cd and Cu in Anyang were higher than those in the other cities. Co, Cr, Ni, V, and Zn were at intermediate levels. The I_{geo} values of Mn and Pb in this study were relatively higher: Mn was lower only than that of sites from Witbank, the largest coal base in South Africa (Zibret et al., 2013), and Pb was lower only than that in the famous industrial city in Southwest China of Panzhihua (Long et al., 2021). The mean I_{geo} values of Zn in the four iron/steel smelting-affected cities were more than 3, showing heavy pollution. Cd and Pb exceeded 2, exhibiting moderate to heavy pollution (Tables S4). Compared with the other types of smelting areas, Co, Cr, and Mn in dust from the iron/steel smelting-affected areas had the highest I_{geo} values. Cd and Cu with high I_{geo} values appeared in the Pb–Zn and Cu smelting areas, respectively, whereas little difference existed in the I_{geo} values of Zn among the three types of smelting areas. The mean I_{geo} values of Cd in the Pb–Zn and Cu smelting-affected cities exceeded 5, which was classified as extremely polluted. A comparison of mean *INI* values among the three types of smelting-affected areas suggested a pollution degree in the following order: Pb–Zn smelter > Cu smelter > iron/steel smelter (Tables S4).

3.2. Source apportionment

Pearson correlation analysis and clustering analysis were initially applied to identify the correlations and similarities in HM concentrations for accurate discrimination among various potential pollution sources. Then, the PMF model was used to quantitatively and qualitatively analyse each pollution source. In the PMF model, collinearity analysis was performed first on the HM concentration data. All HMs with a variance inflation factor greater than 10 and tolerance greater than 0.1 were satisfactory for the analysis requirements (Peng et al., 2021). When the factor number was four, the minimum and stable value of the objective function Q can be derived (Chen et al., 2019). Most residual values fell within the range of −3 to 3, and the minimal R^2 of HMs between measured and predicted values was higher than 0.60, indicating accurate and optimal PMF model result (Zhao et al., 2022). Consequently, four pollution sources were identified, and their contribution rates to HM concentrations are shown in Fig. 4c.

Correlation analysis results indicated strong positive correlations ($0.60 < r < 0.80$, $p < 0.01$) for the pairs Cd–Pb, Cu–Ni, Co–Cu, Co–Ni, Cr–Zn, and Co–Cr, as well as moderate positive correlations ($0.40 < r < 0.60$, $p < 0.01$) for the pairs Cd–Ni, Cd–Zn, Cd–Cu, Cr–Ni, Cu–Pb, Mn–V, and Pb–Zn (Fig. 4a). This result showed that these HMs may originate from a similar source (Jin et al., 2019). Mn and V exhibited negative correlations with other HMs, indicating that their possible sources of contamination were distinct from those of the other elements. Meanwhile, clustering analysis results showed that Cd–Pb, Cu–Co–Ni, Cr–Zn, and Mn–V were clustered (Fig. 4b). Thus, these pairs may share familiar sources (Liu et al., 2019; Sun et al., 2022).

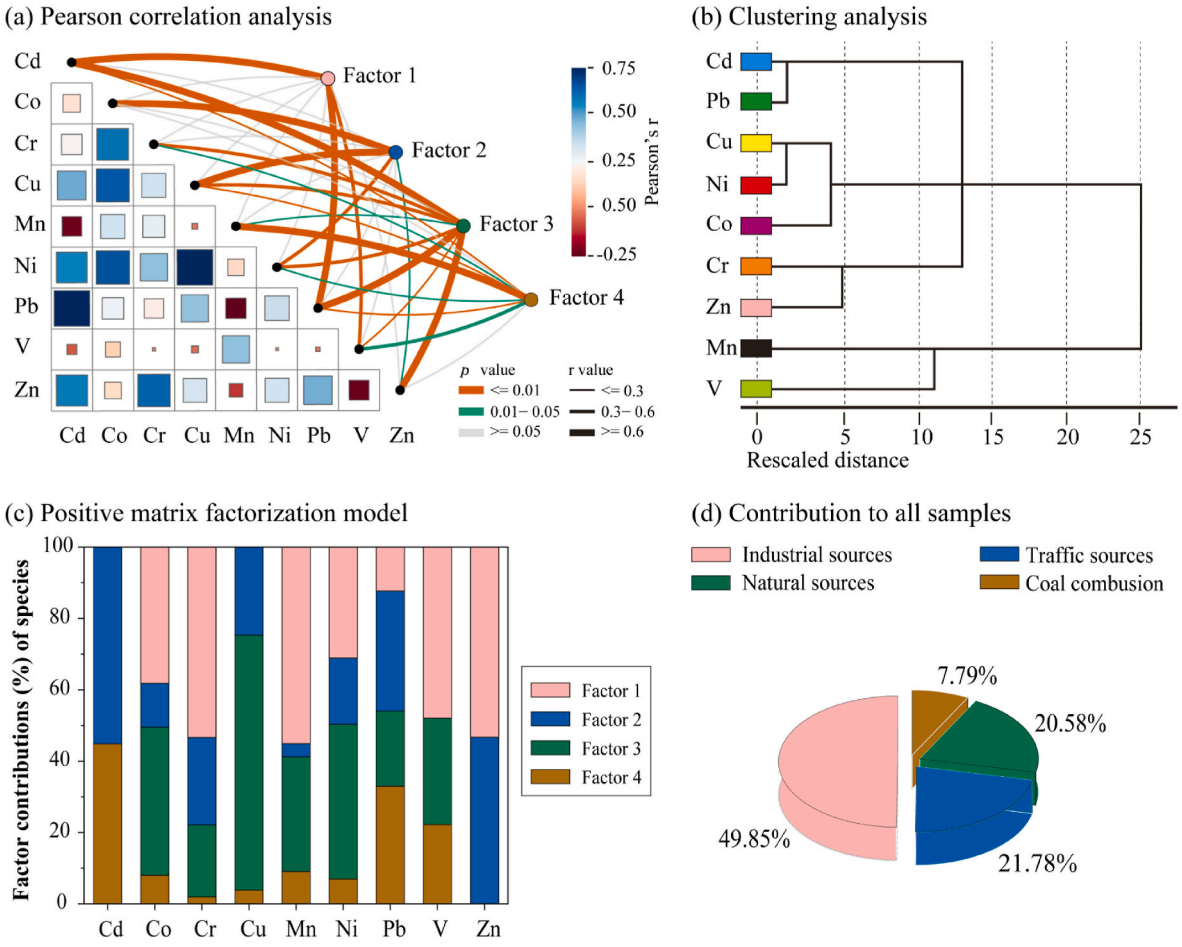

Fig. 4. Source analysis for HMs in windowsill dust: (a) Pearson's correlation coefficient, (b) clustering pattern, (c) factor scores for HMs, and (d) factor contributions to all dust samples.

Factor 1, which explained 49.85% of the overall variance (Fig. 4d), was primarily characterised by Cr (53.30%), Mn (55.11%), V (47.97%), and Zn (53.26%). Many previous investigations have demonstrated that Cr, Mn, V, and Zn are linked to industrial activity (Han et al., 2021a; Soltani et al., 2021). Meanwhile, the strategically valuable element V is extensively used to produce steel alloys (Li et al., 2020a). Ferrovanadium production is estimated to account for about 85% of global V consumption (Yang et al., 2017; Watt et al., 2018). Cr and Mn can be generated and released into the atmosphere along with V during converter smelting (Kelepertzis et al., 2020; Zhang et al., 2022), whereas Zn is extensively used in the galvanising industry to improve steel corrosion resistance and mechanical behaviour (Li et al., 2020b). The leading industries in this study area were iron/steel smelting and related machinery manufacturing. These processes can emit enormous amounts of HM-containing dust (Long et al., 2021). By 2019, more than 200 small- and medium-sized ferroalloy enterprises were located in the northern and western parts of the smelter (AMBS, 2020). Moreover, the GIS map revealed that Mn and V with high concentrations were also primarily concentrated in these regions (Fig. S3). Therefore, Factor 1 was inferred as industrial sources, such as metal smelting and manufacturing machinery.

Factor 2 was allocated to traffic emissions with a contribution rate of 21.78% (Fig. 4d). This factor was primarily loaded on Cd (55.12%), Pb (33.63%), and Zn (46.74%). Significant correlations ($p < 0.01$) were observed between these HMs, indicating common sources (Han et al., 2023). The GIS map also showed that the hotspots for Cd, Pb, and Zn appeared at the main gate of the smelter, an area with a high frequency of transportation activity(Fig. S3). Generally, Cd, Pb, and Zn contamination is typically attributed to traffic activities (Mielke et al., 2011; Ahamad et al., 2021). Although China's nationwide moratorium on leaded gasoline went into effect on July 1, 2000, significant Pb concentrations remain in urban environments due to its half-life of hundreds of years (Jin et al., 2019). Pb has a long history of being widely applied in paint production (Peng et al., 2019). Pb-based coatings have the characteristics of adhesion onto substrates and surfaces (Gilbert and Weiss, 2006), bright colour, and crack resistance (O'Connor et al., 2018). $PbCO_3$ and $PbCrO_4$ are extensively used to mark white and yellow traffic lines, respectively (Peng et al., 2019). Zn and Pb are also reportedly used to produce automobile batteries (Chen et al., 2008; Sun et al., 2022), and Cd is a constituent of tires and lubricants (Li et al., 2001). According to the statistical yearbook of Anyang (AMBS, 2020), road density and vehicle number in 2019 were 69.50 (km/100 km^2) and 955 807, respectively. Increasing vehicle exhaust emissions or tire wear lead to pollution-related elements (Hou et al., 2019). Thus, this factor can be interpreted as traffic sources.

Factor 3, which explained 20.58% of the overall variance (Fig. 4d), had the strongest correlation with Co, Cu, Mn, and Ni (Fig. 4a). Many previous studies have shown that Co, Mn, and Ni may have natural origins (Facchinelli et al., 2001; Egodawatta et al., 2013). The mean concentrations of Co and Ni were close to the regional background values in this work (Fig. S1a), an d their I_{geo} values of 95.65% and 100.00% were classified as unpolluted (Fig. S2b).Notably, many flowers and trees were planted near the sampling windowsills. Cu-containing fungicides and pesticides are commonly used to protect them from pathogenic pathogens and pests (Zhang et al., 2018), leading to Cu accumulation in dust. The spatial distribution of Co, Ni, and Cu concentrations were also relatively uniform (Fig. S3). Consequently, Factor 3 was principally derived from natural sources, accompanied by little contribution from human activities.

Factor 4 may be related to coal combustion, contributing 7.79% of the overall variance (Fig. 4d). This factor was heavily weighted on Cd (44.88%) and Pb (33.01%). A significantly positive correlation existed between Cd and Pb ($r = 0.75$, $p < 0.01$) and the same clustering groups (Fig. 4a–**b**), indicating a similar source of these HMs. Previous studies have reported that in addition to metal smelting, transportation emissions, and waste incineration, fossil-fuel combustion also contributes to Cd enrichment in environmental media (Khan et al., 2016). Remarkably, coal-mining exhaust from fossil fuel was also a significant source of Pb (Sun et al., 2022). Cd and Pb can diffuse into the atmosphere by coal combustion and then into dust through dry and wet atmospheric deposition (Duan et al., 2020). According to statistical data (AMBS, 2020), the Anyang coal-fired power plant, located southwest of the study area, consumed 3.79 million tons of coal in 2019. Therefore, Factor 4 was allocated to the source of coal combustion.

3.3. Bioaccessibilities of HMs

The percentage gastrointestinal bioaccessibilities and total concentrations of HMs in outdoor windowsill dust near the iron/steel smelting-affected areas are presented in Fig. 5 and Table S6. HM bioaccessibilities in all dust samples ranged from 0.02% to 65.16%. The mean bioaccessibilities of HMs decreased as follows: Zn > Pb > Cd > Mn > V > Cu > Ni > Co > Cr for PBETG, and Mn > V > Zn > Ni > Cd > Co > Cu > Pb > Cr for PBETI. Zn, Mn, Cd, and Pb had higher biodetectable concentrations in the gastrointestinal system than other HMs, and Pb had the highest bioaccessibility (65.16%) in PBETG. Cr demonstrated the lowest bioaccessibility, with only 5.27% and 2.04% of Cr in PBETG and PBETI, respectively, being biodetectable. In the present work, Cr was identified primarily from smelting activities, as analysed in Section 3.3. It primarily existed as residue that was not easily digestible by simulated gastrointestinal solution (Piggio et al., 2009; Wang et al., 2019).

The mean bioaccessibilities of all HMs in PBETG exceeded that in PBETI, decreasing by 80.80% (Cd), 44.31% (Co), 61.22% (Cr), 74.40% (Cu), 51.13% (Mn), 25.09% (Ni), 92.14% (Pb), 41.27% (V), and 71.84% (Zn) in PBETI, respectively. Meanwhile, more considerable differences in HM bioaccessibilities were found in PBETG than in PB ETI (Table S6). These results may have been due to the shift in pH of the simulated extract (Kastury et al., 2017; Xing et al., 2020). In PBETG, the pH was 1.5, in which the activity of digestive enzymes increased, resulting in the rapid dissolution of HMs (Zhang et al., 2019). However, the pH in PBETI was 8.0, in which HMs were susceptible to adsorption and precipitation, which passivated and immobilised these HMs in the intestinal fluid (Pelfrene et al., 2011; Aurelie et al., 2011).

Notably, some HMs (Cd, Cr, Pb, and Zn) with high concentrations had low bioaccessibilities in PBETG and PBETI (Fig. 5). These sampling points were located in the southern part of the iron/steel smelting-affected area (S9#–S15#) (Fig. 1), downwind of the prevailing wind direction during the sampling period. On one hand, HM bioaccessibilities in the gastrointestinal system showed little correlation with their concentrations. They were influenced by many factors, such as sampling site (Ma et al., 2021), sources (Liu et al., 2019), sample parameters (e.g., pH, magnetic susceptibility, and particle size), and extraction methods (Ma et al., 2022). On the other hand, bioaccessibility-based health exposure risk results were more accurate and can better reveal the hazards of HMs in dust. Therefore, incorporating the bioaccessibilities into the HHRA model was necessary.

3.4. Health-risk assessment of HMs

3.4.1. Concentration-based risk assessment

Based on the MCS, probabilistic health risks from HMs in windowsill dust within iron/steel smelting-affected areas were characterised (Fig. 6 and Table 1). For children and adults, the average *HQs* of all investigated HMs decreased as follows: Pb > Cr > Mn > V > Cd > Zn > Cu > Ni > Co. The average *HQs* and *HI* of HMs for children were around an order of magnitude greater than those for adults. For adults, the mean *HI* and *HQs* based on the total HM concentrations were less than 1.0, showing negligible noncarcinogenic risks. However, the average *HI* for children was 1.12, which was 1.12 times greater than the safe level. Meanwhile, 59.04% of *HI* for children exceeded 1.0, indicating noncarcinogenic risks (Fig. 6a). In the present work, only Pb, Cr, and Cd were calculated for carcinogenic risks. For children and adults, Cd was proven to be the

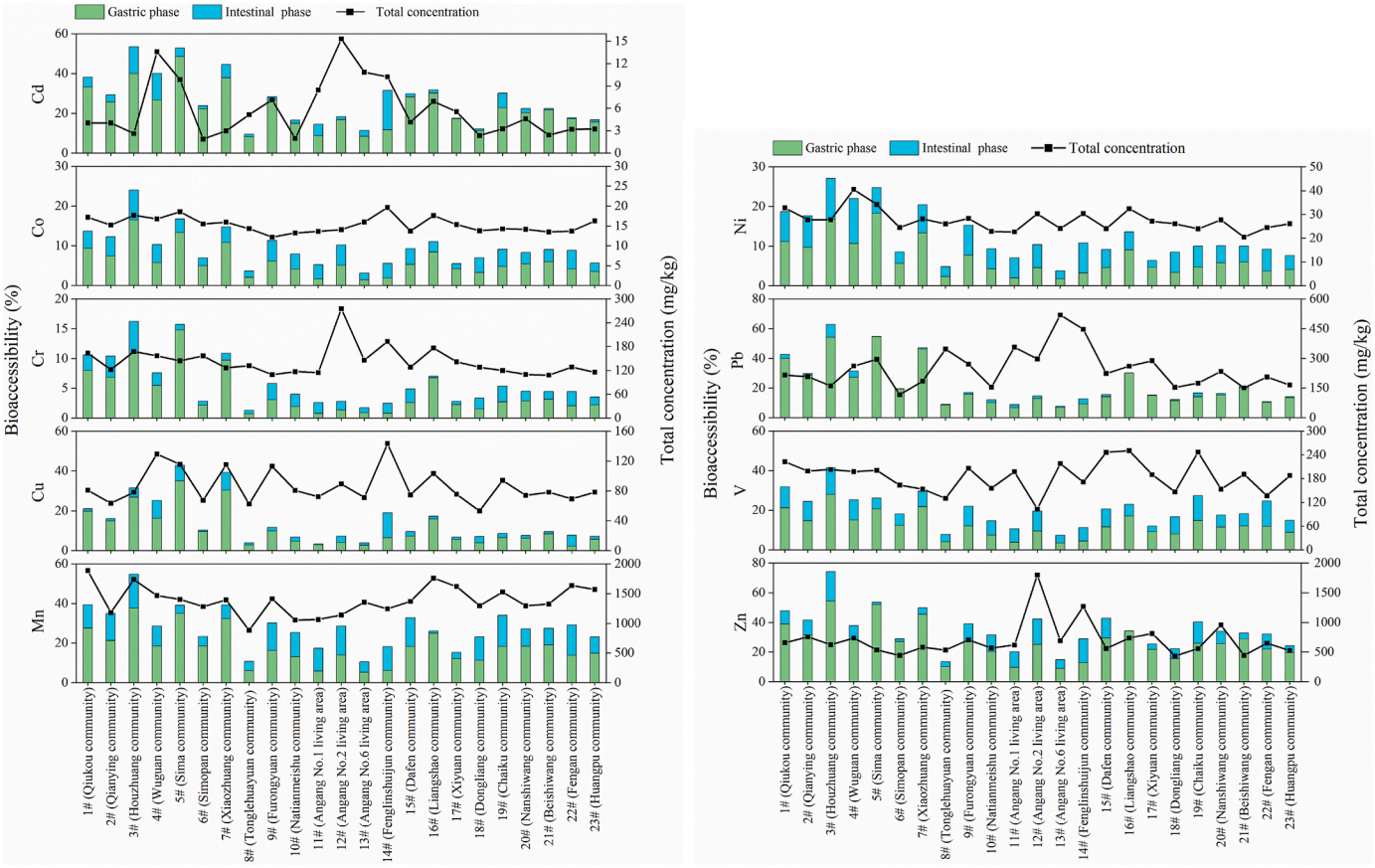

Fig. 5. Percentage bioaccessibilities and total concentrations of HMs in windowsill dust.

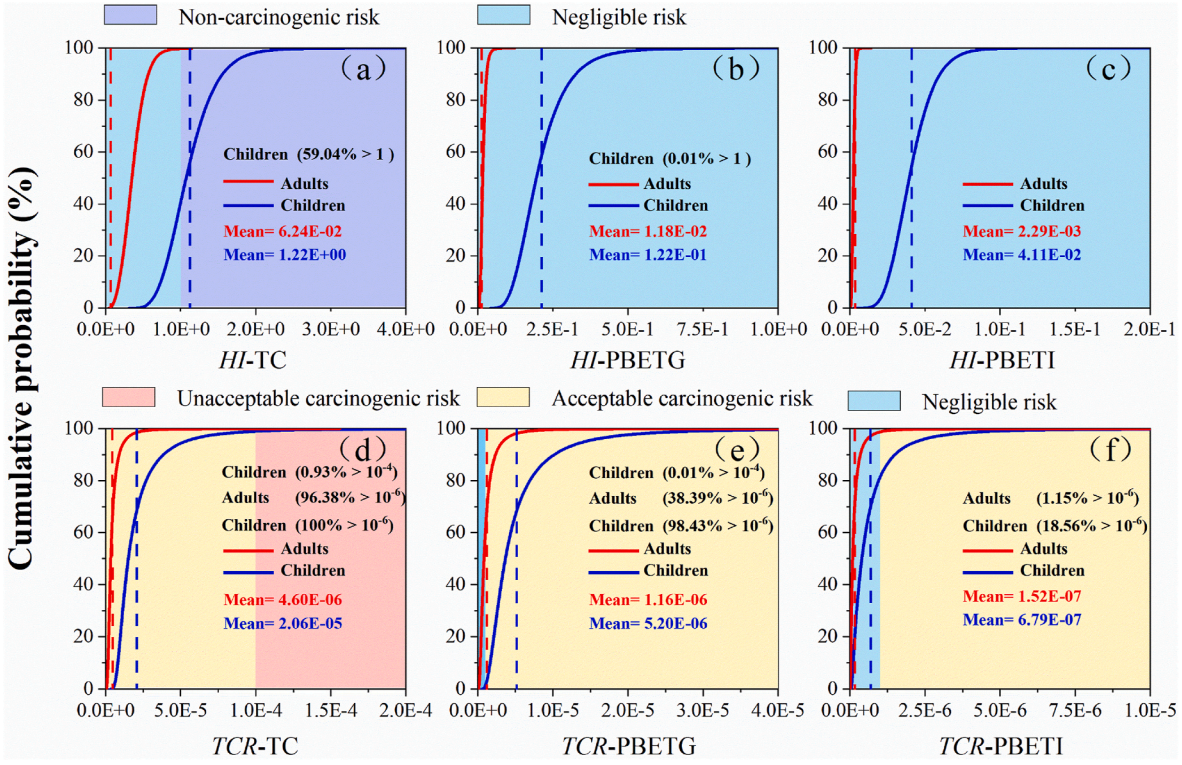

Fig. 6. Probability distributions of concentration- and oral bioaccessibility-based risks (*HI* and *TCR*) of HMs in windowsill dust.

Table 1
Concentration- and oral bioaccessibility-based risks (*HI* and *TCR*) for adults and children of HMs in windowsill dust.

Elements	Children			Adults		
Noncarcinogenic risk: *HQ* and *HI*						
HQ	TC	PBETG	PBETI	TC	PBETG	PBETI
Cd	3.61E-02	9.32E-03	1.26E-03	2.02E-03	5.21E-04	7.07E-05
Co	4.57E-03	3.31E-04	1.65E-04	2.56E-04	1.85E-05	9.23E-06
Cr	2.71E-01	1.57E-02	4.52E-03	1.52E-02	8.77E-04	2.52E-04
Cu	1.29E-02	1.76E-03	4.70E-04	7.18E-04	9.83E-05	2.63E-05
Mn	1.80E-01	3.86E-02	1.61E-02	1.00E-02	2.16E-03	9.01E-04
Ni	8.12E-03	7.34E-04	4.80E-04	4.54E-04	4.11E-05	2.69E-05
Pb	4.24E-01	1.16E-01	3.80E-03	2.37E-02	6.48E-03	2.12E-04
V	1.58E-01	2.32E-02	1.31E-02	8.83E-03	1.30E-03	7.32E-04
Zn	2.09E-02	6.39E-03	1.13E-03	1.16E-03	3.57E-04	6.34E-05
HI	**1.12E+00**	2.12E-01	4.11E-02	6.24E-02	1.18E-02	2.29E-03
Carcinogenic risk: *CR* and *TCR*						
CR	TC	PBETG	PBETI	TC	PBETG	PBETI
Cd	**1.89E-05**	**4.87E-06**	6.59E-07	**4.22E-06**	**1.09E-06**	1.48E-07
Cr	5.92E-07	3.44E-08	9.87E-09	1.32E-07	7.67E-09	2.20E-09
Pb	**1.08E-06**	2.96E-07	9.69E-09	2.42E-07	6.61E-08	2.16E-09
TCR	**2.06E-05**	**5.20E-06**	6.79E-07	**4.60E-06**	**1.16E-06**	1.52E-07

Note: The values that exceed the risk values (*HI*, 1; *TCR*, 1.00E-06) were marked in bold.

dominant factor in the overall carcinogenic risks (Table 1). The mean *TCR* for children and adults were 2.06E-05 and 4.60E-06, respectively, indicating cautionary carcinogenic risks in this study area. Furthermore, 0.93% of *TCR* for children was more than the safe level (>1.0E-04). In comparison, 100.0% and 96.38% of *TCR* for children and adults, respectively, exceeded the acceptable level (>1.0E-06) (Fig. 6d). This result revealed that the carcinogenic risks of HMs, especially Cd, in dust warranted public attention.

3.4.2. Bioaccessibility-based risk assessment

After incorporating HM bioaccessibilities, all *HQ*, *HI*, *CR*, and *TCR* were significantly reduced (Fig. 6 and Table 1). For noncarcinogenic effects, the trend of average *HQs* modified by HM bioaccessibilities for children and adults changed to Pb > Mn > V > Cr > Cd > Zn > Cu > Ni > Co for PBETG and Mn > V > Cr > Pb > Cd > Zn > Ni > Cu > Co for PBETI. Pb and Mn became the dominant contributors to *TCR* posed by biodetectable HMs in PBETG and PBETI, respectively. This inconsistent trend was primarily due to differences in bioaccessibilities and *RfD* values among HMs (Tables S3 and **S6**). In PBETG, although the bioaccessibility of Pb (26.04%) was lower than that of Zn (30.56%), its *RfD* value (3.50E-03) was two orders of magnitude less than that of Zn (3.00E-01), which according to Equation (6) resulted in a higher noncarcinogenic risk. In PBETI, the bioaccessibility of Mn (10.18%) was more five times than that of Pb (2.05%), which can offset the impact of *RfD* differences on the result of health-risk assessment. Additionally, the average *HI* based on HM bioaccessibilities was less than 1.0 for children and adults. Only 0.01% of the *HI* for children exceeded 1.0 (Fig. 6b and **c**). For carcinogenic risks, Cd remained the dominant factor affecting noncarcinogenic risks after adjustment by HM bioaccessibilities in PBETG and PBETI. This consistent trend was primarily due to the high bioaccessibility of Cd an d high *SF* (Tables S3 and **S6**). When incorporating oral bioaccessibilities in PBETG, the mean *TCR* for children (5.20E-06) and adul ts (1.16E-06) remained above 1.0E-06, indicating carcinogenic risks (Fig. 6e and **f**). Particularly, the *TCR* for children between 1.0E-06 and 1.0E-04 was 98.43% (PBETG) and 18.56% (BETGI). Thus, people especially children living around the iron/steel smelting-affected areas need to avoid 'hand-to-mouth' exposure to HMs in dust.

3.4.3. Source-oriented risk assessment

Remarkably, HMs originating from various sources show significantly different concentrations, bioaccessibilities, and toxicity coefficients (Ma et al., 2021), but the traditional concentration-HHRA model cannot effectively distinguish between the effect of natural and anthropogenic sources on health-risk assessment (Sun et al., 2022; Zhao et al., 2022). Thus, source-oriented exposure risks were quantified according to oral bioaccessibilities estimated by PBET and source profiles to identify elevated-risk sources of pollution (Ma et al., 2018; Liu et al., 2019) (Fig. 7). The source-contribution rate (%) to *HI* and *TCR* for children and adults was similar. For noncarcinogenic effects, the *HI* of each pollution source, as analysed in Section 3.3, were lower than 1.0, suggesting negligible noncarcinogenic risks (Table 2). Among them, Factor 1 (industrial sources) which accounted for 49.85% of all pollution sources were primarily loaded on Cr, Mn, V, and Zn, and it had the highest contribution rate (total concentration: 34.69%; PBETG: 27.74%; PBETI: 45.95%) to the noncarcinogenic risks (Fig. 7). This finding may be correlated with the high bioaccessibilities of Mn, V, and Zn in the gastrointestinal system and the low noncarcinogenic toxicity of Cr (Tables S3 and **S6**). Thus, industrial source was determined as a crucial pollution source of the noncarcinogenic effects. In terms of carcinogenic effects, industrial sources and natural sources explained 49.85% and 20.58% of all pollution sources, respectively, but the contribution rates of these two anthropogenic sources to *TCR* were below 5%. It was primarily due to the low loading on Cd and Pb and low bioaccessibility of Cr in PBETG and PBETI (Tables S3 and **S6**). Although industrial sources had a low contribution rate of posing carcinogenic risk to the population, more prevention and control policies were still needed to reduce the risk caused by HMs, especially the potentially carcinogenic element Cd. The concentration-based *TCR* and PBETG-based *TCR* for children and adults of Factor 2 (traffic sources) and Factor 4 (coal combustion) were above or close to 1.0E-06 (Table 2), suggesting the existence of carcinogenic risks. Although traffic sources and coal combustion accounted for only 21.78% and 7.79% of all pollution sources, respectively, these two sources became the more significant risk sources for carcinogenic risks with a contribution rate of more than 40% (Fig. 7), consistent with Huang et al. (2018) and Ma et al. (2021). It was primarily due to traffic sources and coal combustion having high allocations of Cd and Pb (Fig. 4). Hence, traffic sources and Cd were identified as crucial pollution sources and key pollution factors for the carcinogenic effects.

As discussed above, iron/steel smelting and related production and transportation activities were the prerequisite for minimising the influx of new HMs and the associated health risks in the study area. Accordingly, the emission standard of air pollutants, including measures to lower discharge limits and transportation-related and industry-related emissions, was necessary and should be enforced first. Then, air pollutant emission detection and risk-based management should be performed on a point-by-point basis. However, the economic development of small- and medium-sized cities is primarily driven by increasing energy consumption and industrial production activities, especially for China's industrial-oriented cities (Zhang et al., 2019). Considering sustainable development, we advocate the use of new energy sources instead of fossil fuels in industrial-production activities. Notably, China's fossil energy peaked in 2010 (accounting for nearly 92% of the total energy consumption) and has shown a downward trend in recent years (NBS, 2020), indicating that city managers have consciously reduced the use of fossil energy in green production and energy

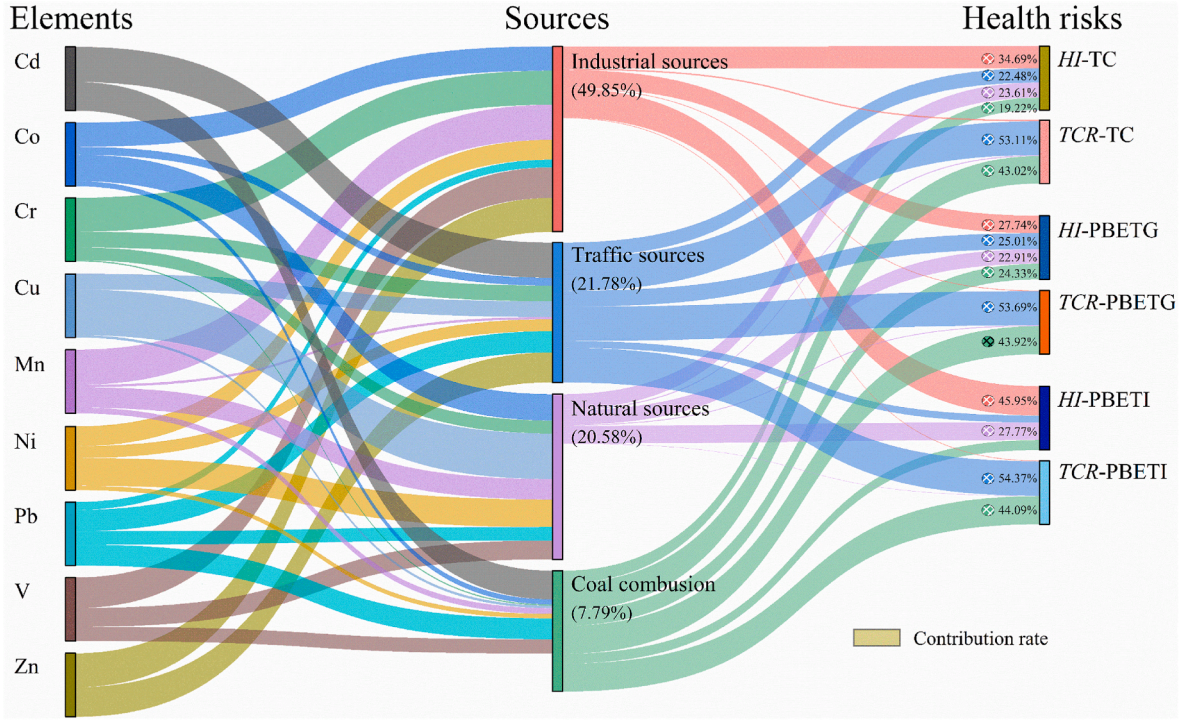

Fig. 7. Summary of source contribution (%) to concentration- and oral bioaccessibility-based risks (*HI* and *TCR*) of HMs in windowsill dust.

Table 2
Source-oriented health risks for adults and children according to the concentration- and oral bioaccessibility-based risks (*HI* and *TCR*) of HMs in windowsill dust.

Elements	Children				Adults			
	Factor 1	Factor 2	Factor 3	Factor 4	Factor 1	Factor 2	Factor 3	Factor 4
Noncarcinogenic risk: hazard index (*HI*)								
TC	2.14E-01	2.51E-01	2.63E-01	2.14E-01	2.16E-02	1.40E-02	1.47E-02	1.20E-02
PBETG	5.16E-02	5.31E-02	4.86E-02	5.16E-02	3.29E-03	2.96E-03	2.71E-03	2.88E-03
PBETI	6.35E-03	4.44E-03	1.14E-02	6.35E-03	1.05E-03	2.48E-04	6.37E-04	3.55E-04
Carcinogenic risk: total carcinogenic risk (*TCR*)								
TC	4.49E-07	**1.09E-05**	3.47E-07	**8.85E-06**	1.00E-07	**2.44E-06**	7.77E-08	**1.98E-06**
PBETG	5.48E-08	**2.79E-06**	6.92E-08	**2.28E-06**	1.22E-08	6.25E-07	1.55E-08	5.11E-07
PBETI	6.46E-09	3.69E-07	4.04E-09	2.99E-07	1.44E-09	8.27E-08	9.00E-10	6.71E-08

Note: Factor 1: industrial sources, Factor 2: traffic sources, Factor 3: natural sources, Factor 4: coal combustion. The values that exceed the risk values (*HI*, 1; *TCR*, 1.00E-06) were marked in bold.

management. Overall, our research highlighted that source-oriented health-risk assessment was more effective for the identification of crucial pollution sources and key pollution factors than other methods based on total HM concentrations.

4. Conclusions

The average concentrations of all HMs (except for Ni) in outdoor windowsill dust samples exceeded the regional background values from soil in Henan Province, whereas only Cr and V had average concentrations that were more elevated than the relevant soil risk-control standards. Cd had the highest average I_{geo}, exhibiting heavy to extreme pollution and extreme pollution. Source apportionment indicated that industrial sources (49.85%) were significant sources of HMs in dust within the iron/steel smelting-affected areas, followed by traffic sources (21.78%), natural sources (20.58%), and coal combustion (7.79%). The mean bioaccessibility values of most HMs (except Zn) determined by PBET tests were less than 30% and exhibited significant variation between PBETG and PBETI. When considering HM oral bioaccessibilities, noncarcinogenic and carcinogenic risks were significantly reduced, especially for adults. The priority HM contaminant changed from Pb (total concentration) to Mn (PBETI) for noncarcinogenic risks, whereas Cd was consistently identified as the critical pollution factor for carcinogenic effects. Industrial and traffic sources were high-risk sources of concern that contributed the most to the *HI* and *TCR* values. This work generally reconfirmed the necessity of incorporating bioaccessibility rather than the total concentration for the source-oriented health-risk assessment of HMs. These findings provided more applicable information for the health-risk assessment and contamination control of HMs within iron/steel smelting-affected areas.

Credit authors statement

Mingya Wang: Formal analysis, Writing – original draft preparation. **Xiaohang Xu**: Conceptualization, Writing – review & editing. **Qiao Han**: Literature collection, Supervision, Project administration, Writing – review & editing. **Xihuang Lin** and **Haijun Yuan**: Methodology, Writing – review & editing. **Fengcheng Jiang** and **Mingshi Wang**: Resources, Funding acquisition. **Wenju Wang**: Investigation, Data curation.

Declaration of competing interest

The authors declare that they have no known competing financial interests or personal relationships that could have appeared to influence the work reported in this paper.

Data availability

Data will be made available on request.

Acknowledgments

This work was supported by the Strategic Priority Research Program of the Chinese Academy of Sciences (XDB40020405) and Henan Province Key Science and Technology Research Projects (222102320102).

Appendix A. Supplementary data

Supplementary data to this article can be found online at https://doi.org/10.1016/j.envres.2023.117101.

References

Ahamad, A., Raju, N.J., Madhav, S., Gossel, W., Ram, P., Wycisk, P., 2021. Potentially toxic elements in soil and road dust around sonbhadra industrial region, Uttar Pradesh, India: source apportionment and health risk assessment. Environ. Res. 202, 11685.

AMBS (Anyang City Municipal Bureau of Statistics), 2020. Anyang City Statistical Yearbook in 2020. China Statistics Press, Beijing (In Chinese).

Aurelie, Pelfrene, Waterlot, C., Mazzuca, M., Nisse, C., Bidar, Geraldine, Douay, F., 2011. Assessing Cd, Pb, Zn human bioaccessibility in smelter-contaminated agricultural topsoils (Northern France). Environ. Geochem. Health 33 (5), 477–493.

Berasaluce, M., Mondaca, P., Schuhmacher, M., Bravo, M., Sauve, S., Navarro-Villarroel, C., Dovletyarova, E.A., Neaman, A., 2019. Soil and indoor dust as environmental media of human exposure to as, cd, cu, and pb near a copper smelter in central Chile. J. Trace Elem. Med. Biol. 54, 156–162.

Cao, S.Z., Chen, X., Zhang, L.L., Xing, X.R., Wen, D.S., Wang, B.B., Qin, Ning, Wei, F.S., Duan, X.L., 2020. Quantificational exposure, sources and health risks posed by heavy metals in indoor and outdoor household dust in a typical smelting area in China. Indoor Air 30 (5), 872–884.

Chen, R.H., Chen, H.Y., Song, L.T., Yao, Z.P., Meng, F.S., Teng, Y.G., 2019. Characterization and source apportionment of heavy metals in the sediments of Lake Tai (China) and its surrounding soils. Sci. Total Environ. 694, 133819.

Chen, T., Liu, X.M., Zhu, M.Z., Zhao, K.L., Wu, J.J., Xu, J.M., Huang, P.M., 2008. Identification of trace element sources and associated risk assessment in vegetable soils of the urban–rural transitional area of Hangzhou, China. Environ. Pollut. 151, 67–78.

CNEMC (China National Environmental Monitoring Centre), 1990. The Soil Background Value in China. China Environmental Science Press, Beijing (In Chinese).

Delbeke, K., Baken, S., Simbor, L.P., Rodriguez, P.H., Brouwers, T., Verougstraete, V., Binks, S., Oller, A., Danzeisen, R., Gilles, M., 2020. Copper alloys' metal migration and bioaccessibility in saliva and gastric fluid. Regul. Toxicol. Pharmacol. 117, 104754.

Dong, L., Zhang, H., Fujita, T., Ohnishi, S., Li, H.Q., Fujii, M., Dong, H.J., 2013. Environmental and economic gains of industrial symbiosis for Chinese iron/steel industry: kawasaki's experience and practice in Liuzhou and Jinan. J. Clean. Prod. 59 (15), 226–238.

Duan, Y.X., Zhang, Y.M., Li, S., Fang, Q.L., Miao, F.F., Lin, Q.G., 2020. An integrated method of health risk assessment based on spatial interpolation and source apportionment. J. Clean. Prod. 276, 123218.

Egodawatta, P., Ziyath, A.M., Goonetilleke, A., 2013. Characterising metal build-up on urban road surfaces. Environ. Pollut. 176, 87–91.

Facchinelli, A., Sacchi, E., Mallen, L., 2001. Multivariate statistical and GIS-based approach to identify heavy metal sources in soils. Environ. Pollut. 114, 313–324.

Feng, Y.Y., Shi, J.W., Zhong, Y.Q., Han, X.Y., Feng, Y.C., Ren, L., 2020. Pollution characteristics and health risk assessment of heavy metals in road dust from non-ferrous smelting parks. Environ. Sci. J. Integr. Environ. Res. 1–13 (In Chinese).

Fry, K.L., Gillings, M.M., Isley, C.F., Gunkel-Grillon, P., Taylor, M.P., 2021. Trace element contamination of soil and dust by a New Caledonian ferronickel smelter: dispersal, enrichment, and human health risk. Environ. Pollut. 288 (1), 117593.

Ganyaglo, S.Y., Gibrilla, A., Teye, E.M., Owusu-Ansah, E.D.-G.J., Tettey, S., Diabene, P. Y., Asimah, S., 2019. Groundwater fluoride contamination and probabilistic health risk assessment in fluoride endemic areas of the upper east region, Ghana. Chemosphere 233, 862–872.

Gilbert, S.G., Weiss, B., 2006. A rationale for lowering the blood lead action level from 10 to 2mg/dL. Neurotoxicology 27, 693–701.

Gu, Y.G., Gao, Y.P., 2018. Bioaccessibilities and health implications of heavy metals in exposed-lawn soils from 28 urban parks in the megacity Guangzhou inferred from an *in vitro* physiologically-based extraction test. Ecotoxicol. Environ. Saf. 148, 747–753.

Han, C.L., Xu, R.B., Gao, C.X., Yu, W.H., Zhang, Y.J., Han, K., Yu, P., Guo, Y.M., Li, S.S., 2021b. Socioeconomic disparity in the association between long-term exposure to $PM_{2.5}$ and mortality in 2640 Chinese counties. Environ. Int. 146, 106241.

Han, J.L., Liang, L.C., Zhu, Y.R., Xu, X.H., Wang, L., Shang, L.H., Wu, P., Wu, Q.X., Qian, X.L., Qiu, G.L., Feng, X.B., 2022. Heavy metal(loid)s in farmland soils on the Karst Plateau, Southwest China: an integrated analysis of geochemical baselines, source apportionment, and associated health risk. Land Degrad. Dev. 33, 1689–1703.

Han, Q., Liu, Y., Feng, X.X., Mao, P., Sun, A., Wang, M.Y., Wang, M.S., 2021a. Pollution effect assessment of industrial activities on potentially toxic metal distribution in windowsill dust and surface soil in Central China. Sci. Total Environ. 759, 144023.

Han, Q., Wang, M.S., Cao, J.L., Gui, C.L., Liu, Y.P., He, X.D., He, Y.C., Liu, Y., 2020. Health risk assessment and bioaccessibilities of heavy metals for children in soil and dust from urban parks and schools of Jiaozuo, China. Ecotoxicol. Environ. Saf. 191, 110157.

Han, Q., Wang, M.Y., Xu, X.H., Li, M.F., Liu, Y., Zhang, C.H., Li, S.H., Wang, M.S., 2023. Health risk assessment of heavy metals in road dust from the fourth-tier industrial city in central China based on Monte Carlo simulation and bioaccessibility. Ecotoxicol. Environ. Saf. 252, 114627.

Hou, S.G., Zheng, N., Tang, L., Ji, X.F., Li, Y.Y., Hua, X.Y., 2019. Pollution characteristics, sources, and health risk assessment of human exposure to Cu, Zn, Cd and Pb pollution in urban street dust across China between 2009 and 2018. Environ. Int. 128, 430–437.

Huang, J.L., Wu, Y.Y., Sun, J.X., Li, X., Geng, X.L., Zhao, M.L., Sun, T., Fan, Z.Q., 2021. Health risk assessment of heavy metal(loid)s in park soils of the largest megacity in China by using Monte Carlo simulation coupled with Positive matrix factorization model. J. Hazard Mater. 415, 125629.

Huang, R.J., Cheng, R., Jing, M., Yang, L., Li, Y.J., Chen, Q., Chen, Y., Yan, J., Lin, C.S., Wu, Y.F., Zhang, R.J., Haddad, I.E., Prevot, A.S.H., O'Dowd, C.D., Cao, J.J., 2018. Source-specific health risk analysis on participate trace elements: coal combustion and traffic emission as major contributors in wintertime Beijing. Environ. Sci. Technol. 52 (19), 10967–10974.

Jeong, H., Choi, J.Y., Ra, K.T., 2021. Potentially toxic elements pollution in road deposited sediments around the active smelting industry of Korea. Sci. Rep. 11, 7238.

Jin, Y.l., David, O., Yong, S.O., Daniel, C.W.T., An, L., Hou, D.Y., 2019. Assessment of sources of heavy metals in soil and dust at children's playgrounds in Beijing using GIS and multivariate statistical analysis. Environ. Int. 124, 320–328.

Juhasz, A.L., Weber, J., Naidu, R., Gancarz, D., Rofe, A., Todor, D., Smith, E., 2010. Determination of cadmium relative bioavailability in contaminated soils and its prediction using in vitro methodologies. Environ. Sci. Technol. 1 44 (13), 5240–5247.

Kastury, F., Smith, E., Juhasz, A.L., 2017. A critical review of approaches and limitations of inhalation bioavailability and bioaccessibility of metal(loid)s from ambient particulate matter or dust. Sci. Total Environ. 574, 1054–1074.

Kastury, F., Smith, E., Karna, R.R., Scheckel, K.G., Juhasz, A.L., 2018. An inhalation-ingestion bioaccessibility assay (IIBA) for the assessment of exposure to metal (loid)s in PM_{10}. Sci. Total Environ. 631–632, 92–104.

Kelepertzis, E., Argyraki, A., Chrastn, V., Botsou, F., Fouskas, A., Skordas, K., Komarek, M., Fouskas, A., 2020. Metal(loid) and isotopic tracing of pb in soils, road and house dusts from the industrial area of Volos (central Greece). Sci. Total Environ. 725, 138300.

Khan, S., Munir, S., Sajjad, M., Li, G., 2016. Urban park soil contamination by potentially harmful elements and human health risk in Peshawar City, Khyber Pakhtunkhwa, Pakistan. J. Geochem. Explor. 165, 102–110.

Li, X., Poon, C., Liu, P.S., 2001. Heavy metal contamination of urban soils and street dusts in Hong Kong. Appl. Geochem. 16, 1361–1368.

Li, Y., Yuan, Y., Sun, C., Sun, T., Liu, X., Li, J., Fang, L., Fan, Z., 2020b. Heavy metals in soil of an urban industrial zone in a metropolis: risk assessment and source apportionment. Stoch. Environ. Res. Risk Assess. 34, 435–446.

Li, Y.N., Zhang, B.G., Liu, Z.Q., Wang, S., Yao, J., Borthwick, A.G.L., 2020a. Vanadium contamination and associated health risk of farmland soil near smelters throughout China. Environ. Pollut. 263, 114540.

Liu, J., Liu, Y.J., Liu, Y., Liu, Z., Zhang, A.N., 2018. Quantitative contributions of the major sources of heavy metals in soils to ecosystem and human health risks: a case study of Yulin, China. Ecotoxicol. Environ. Saf. 164, 261–269.

Liu, J., Zhang, A., Chen, Y., Zhou, X., Zhou, A., Cao, H., 2021a. Bioaccessibility, source impact and probabilistic health risk of the toxic metals in $PM_{2.5}$ based on lung fluids test and Monte Carlo simulations. J. Clean. Prod. 283, 124667.

Liu, L.L., Liu, Q.Y., Ma, J., Wu, H.W., Qu, Y.J., Gong, Y.W., Yang, S.H., An, Y.F., Zhou, Y. Z., 2020. Heavy metal(loid)s in the topsoil of urban parks in Beijing, China: concentrations, potential sources, and risk assessment. Environ. Pollut. 260, 114083.

Liu, X.L., Ouyang, W.Y., Shu, Y.L., Tian, Y.Z., Feng, Y.H., Zhang, T., Chen, W., 2019. Incorporating bioaccessibility into health risk assessment of heavy metals in particulate matter originated from different sources of atmospheric pollution. Environ. Pollut. 254, 113113.

Liu, Y., Wang, M.Y., Ning, P., Han, Q., Wang, M.S., Meng, H.Q., 2021b. Characteristics of $PM_{2.5}$ pollution and source apportionment during winter sampling campaigns in Anyang City. Environmental Monitoring in China 37 (5), 83–93 (In Chinese).

Long, Z.J., Zhu, H., Bing, H.J., Tian, X., Wang, Z.G., Wang, X.F., Wu, Y.H., 2021. Contamination, sources and health risk of heavy metals in soil and dust from different functional areas in an industrial city of Panzhihua City, Southwest China. J. Hazard Mater. 420, 126638.

Luo, C.L., Liu, C.P., Wang, Y., Liu, X., Li, F.B., Zhang, G., Li, X.D., 2011. Heavy metal contamination in soil and vegetables near an e-waste processing site, South China. J. Hazard Mater. 186, 481–490.

Ma, J.J., Yan, Y., Chen, X.J., Niu, Z.R., Yu, R.L., Hu, G.R., 2021. Incorporating bioaccessibility and source apportionment into human health risk assessment of heavy metals in urban dust of Xiamen, China. Ecotoxicol. Environ. Saf. 228, 112985.
Ma, W.C., Tai, L.Y., Qiao, Z., Zhong, L., Wang, Z., Fu, K.X., Chen, G.Y., 2018. Contamination source apportionment and health risk assessment of heavy metals in soil around municipal solid waste incinerator: a case study in North China. Sci. Total Environ. 631–632, 348–357.
Ma, X.Y., Xia, D.S., Liu, X.Y., Liu, H., Fan, Y.J., Chen, P.Y., Yu, Q., 2022. Application of magnetic susceptibility and heavy metal bioaccessibility to assessments of urban sandstorm contamination and health risks: case studies from Dunhuang and Lanzhou, Northwest China. Sci. Total Environ. 830, 154801.
MEE (Ministry of Ecology and Environment), 2018. GB 36600-2018, Soil Quality Standard: Risk Control Standard for Soil Contamination of Development Land. Ministry of Ecology and Environment (In Chinese).
Mehta, N., Cipullo, S., Cocerva, T., Coulon, F., Dion, G.A., Ajmone-Marsan, F., Padoan, E., Cox, S.F., Cave, M.R., Luca, D.A.D., 2020. Incorporating oral bioaccessibility into human health risk assessment due to potentially toxic elements in extractive waste and contaminated soils from an abandoned mine site. Chemosphere 255, 126927.
Mielke, H.W., Laidlaw, M.A., Gonzales, C.R., 2011. Estimation of leaded (Pb) gasoline's continuing material and health impacts on 90 US urbanized areas. Environ. Int. 37, 248–257.
Chinese Statistical Yearbook in 2020, 2020 (In Chinese).
Ning, Z.P., Liu, E.G., Yao, D.J., Xiao, T.F., Ma, L., Liu, Y.Z., Li, H., Liu, C.S., 2021. Contamination, oral bioaccessibility and human health risk assessment of thallium and other metal(loid)s in farmland soils around a historic Tl\Hg mining area. Sci. Total Environ. 758, 143577.
O'Connor, D., Hou, D.Y., Ye, J., Zhang, Y.H., Ok, Y.S., Song, Y.N., Coulon, F., Peng, T.Y., Tian, L., 2018. Lead-based paint remains a major public health concern: a critical review of global production, trade, use, exposure, health risk, and implications. Environ. Int. 121, 85–101.
Paatero, P., Tapper, U., 1994. Positive matrix factorization: a non-negative factor model with optimal utilization of error estimates of data values. Environmetrics 5 (2), 111–126.
Pan, W., Kang, Y., Zeng, L., Zhang, Q., Luo, J., Wong, M.H., 2016. Comparison of *in vitro* digestion model with *in vivo* relative bioavailability of BDE-209 in indoor dust and combination of *in vitro* digestion/Caco-2 cell model to estimate the daily intake of BDE-209 via indoor dust. Environ. Pollut. 218, 497–504.
Pelfrene, A., Waterlot, C., Mazzuca, M., Nisse, C., Bidar, G., Douay, F., 2011. Assessing Cd, Pb, Zn human bioaccessibility in smelter-contaminated agricultural topsoils (Northern France). Environ. Geochem. Health 33 (5), 477–493.
Peng, T.Y., O'Connor, D., Zhao, B., Jin, Y.L., Zhang, Y.H., Tian, L., Zheng, N., Li, X.P., Hou, D.Y., 2019. Spatial distribution of lead contamination in soil and equipment dust at children's playgrounds in Beijing, China. Environ. Pollut. 159, 2320–2327.
Peng, X., Zhang, L., Li, Y., Lin, Q.W., He, C., Huang, S.Z., Li, H., Zhang, X.Y., Liu, B.Y., Ge, F.J., Zhou, Q.H., Zhang, Y., Wu, Z.B., 2021. The changing characteristics of phytoplankton community and biomass in subtropical shallow lakes: coupling effects of land use patterns and lake morphology. Water Res. 200 (15), 117235.
Piggio, L., Vrscaj, B., Schulin, R., Hepperle, E., Marsan, F.A., 2009. Metals pollution and human bioaccessibility of topsoils in Grugliasco (Italy). Environ. Pollut. 152, 680–689.
Ruby, M.V., Andy, Davis, Schoof, Rosalind, Eberle, Steve, Sellstone, Christopher M., 1996. Estimation of lead and arsenic bioavailability using a physiologically based extraction test. Environ. Sci. Technol. 30 (2), 422–430.
Ruby, M.V., Schoof, R., Brattin, W., Goldade, M., Post, G., Harnois, M., Mosby, D.E., Casteel, S.W., Berti, W., Carpenter, M., Edwards, D., Cragin, D., Chappell, W., 1999. Advances in evaluating the oral bioavailability of inorganics in soil for use in human health risk assessment. Environ. Sci. Technol. 33 (31), 3697–3705.
Soltani, N., Keshavarzi, B., Moore, F., Cave, M., Sorooshian, A., Mahmoudi, M.R., Ahmadi, M.R., Golshani, R., 2021. *In vitro* bioaccessibility, phase partitioning, and health risk of potentially toxic elements in dust of an iron mining and industrial complex. Ecotoxicol. Environ. Saf. 212, 111972.
Song, Z.C., Wang, C., Ding, L., Chen, M., Hu, Y.X., Li, P., Zhang, L.M., Feng, X.B., 2021. Soil mercury pollution caused by typical anthropogenic sources in China: evidence from stable mercury isotope measurement and receptor model analysis. J. Clean. Prod. 288, 125687.
Sun, J.X., Zhao, M.L., Huang, J.L., Liu, Y.F., Wu, Y.Y., Cai, B.Y., Han, Z.W., Huang, H.H., Fan, Z.Q., 2022. Determination of priority control factors for the management of soil trace metal(loid)s based on source-oriented health risk assessment. J. Hazard Mater. 432, 127116.
USEPA, 1989. Risk Assessment Guidance for Superfund Volume I: Human Health Evaluation Manual (Part A). U.S. Environment Protection Agency, Washington DC).
USEPA, 2009. Risk Assessment Guidance for Superfund (RAGS). U.S. Environment Protection Agency, Washington DC).
USEPA, 2011. Exposure Factors Handbook, Final. U.S. Environment Protection Agency, Washington DC).
Wang, C.C., Zhang, Q.C., Kang, S.G., Li, M.Y., Zhang, M.Y., Xu, W.M., Xiang, P., Ma, L.Q., 2023. Heavy metal(loid)s in agricultural soil from main grain production regions of China: bioaccessibility and health risks to humans. Sci. Total Environ. 858, 159819.
Wang, G., Diao, J., Liu, L., Li, M., Li, H.Y., Li, G., Xie, B., 2019. Highly efficient utilization of hazardous vanadium extraction tailings containing high chromium concentrations by carbothermic reduction. J. Clean. Prod. 237, 117832.
Wang, H.Z., Cai, L.M., Wang, S., Hu, G.C., Chen, L.G., 2021. A comprehensive exploration on pollution characteristics and health risks of potentially toxic elements in indoor dust from a large Cu smelting area, Central China. Environ. Sci. Pollut. R. 28, 57569–57581.
Watt, J.A.J., Burke, I.T., Edwards, R.A., Malcolm, H.M., Mayes, W.M., Olszewska, J.P., Pan, G., Graham, M.C., Heal, K.V., Rose, N.L., Turner, S.D., Spears, B.M., 2018. Vanadium: a re-emerging environmental hazard. Environ. Sci. Technol. 52 (21), 11973–11974.
Wei, Y., Zheng, X., Zhang, Z., Liang, H., Gu, M., Shen, F., Shohag, M.J.I., Li, X., 2021. *In vivo-In vitro* correlations for the assessment of Cadmium bioavailability in vegetables. J. Agric. Food Chem. 69 (41), 12295–12304.
WSA (World Steel Association), 2020. Steel Statistical Yearbook in 2020.
WSA (World Steel Association), 2021. List of Companies with Tonnage of More than 3 Million Tonnes (Mt) in 2020.
Wu, T.T., Bi, X.Y., Li, Z.G., Sun, G.Y., Feng, X.B., Shang, L.H., Zhang, H., He, T.R., Chen, J., 2017. Contaminations, sources, and health risks of trace metal(loid)s in street dust of a small city impacted by artisanal Zn smelting activities. Int. J. Environ. Res. Publ. Health 14 (9), 961.
Xiao, Q., Zong, Y.T., Malik, Z., Lu, S.G., 2020. Source identification and risk assessment of heavy metals in road dust of steel industrial city (Anshan), Liaoning, Northeast China. Hum. Ecol. Risk Assess. 26 (5), 1359–1378.
Xing, W.Q., Luo, J., Ippolito, J.A., Lu, R.L., Hao, Z.Y., Li, L.P., 2022. Metal contamination in soils and windowsill dusts: implication of multiple sources on dust metal accumulation within a city affected by Pb smelting. Environ. Sci. Pollut. R. 1–13.
Xing, W.Q., Yang, H., Ippolito, J.A., Zhang, Y.Q., Scheckel, K.G., Li, L.P., 2020. Lead source and bioaccessibility in windowsill dusts within a Pb smelting-affected area. Environ. Pollut. 226, 115110.
Yadav, I.C., Devi, N.L., Singh, V.K., Li, J., Zhang, G., 2019. Spatial distribution, source analysis, and health risk assessment of heavy metals contamination in house dust and surface soil from four major cities of Nepal. Chemosphere 218, 1100–1113.
Yan, R.H., Peng, X., Lin, W., He, L.Y., Wei, F.H., Tang, M.X., Huang, X.F., 2022. Trends and challenges regarding the source-specific health risk of $PM_{2.5}$-bound metals in a Chinese megacity from 2014 to 2020. Environ. Sci. Technol. 56 (11), 6996–7005.
Yang, J., Teng, Y.G., Wu, J., Chen, H.Y., Wang, G.Q., Song, L.T., Yue, W.F., Zuo, R., Zhai, Y.Z., 2017. Current status and associated human health risk of vanadium in soil in China. Chemosphere 171, 635–643.
Zahran, S., Laidlaw, M.A.S., McElmurry, S.P., Filippelli, G.M., Taylor, M., 2013. Linking source and effect: resuspended soil Lead, air Lead, and children's blood lead levels in Detroit, Michigan. Environ. Sci. Technol. 47 (6), 2839–2845.
Zgobicki, W., Telecka, M., Skupinski, S., 2019. Assessment of short-term changes in street dust pollution with heavy metals in Lublin (*E* Poland)-levels, sources and risks. Environ. Sci. Pollut. Res. 26, 35049–35060.
Zhang, B., Wang, R.F., Liu, C.J., Jiang, M.F., 2022. Self-digestion of Cr-bearing vanadium slag processing residue via hot metal pre-treatment in steelmaking process. Metall. Mater. Trans. B 53, 1183.
Zhang, H., Mao, Z., Huang, K., Wang, X., Cheng, L., Zeng, L., Zhou, Y., Jing, T., 2019. Multiple exposure pathways and health risk assessment of heavy metal (loid) s for children living in fourth-tier cities in Hubei Province. Environ. Int. 129, 517–524.
Zhang, P., Qin, C., Hong, X., Kang, G., Qin, M., Yang, D., Pang, B., Li, Y., He, J., Dick, R. P., 2018. Risk assessment and source analysis of soil heavy metal pollution from lower reaches of Yellow River irrigation in China. Sci. Total Environ. 633, 1136–1147.
Zhao, Z.J., Hao, M., Li, Y.L., Li, S.H., 2022. Contamination, sources and health risks of toxic elements in soils of karstic urban parks based on Monte Carlo simulation combined with a receptor model. Sci. Total Environ. 839, 156223.
Zia, M.H., Codling, E.E., Scheckel, K.G., Chaney, R.L., 2011. *In vitro* and in *vivo* approaches for the measurement of oral bioavailability of lead (Pb) in contaminated soils: a review. Environ. Pollut. 159, 2320–2327.
Zibret, G., Tonder, D.V., Zibret, L., 2013. Metal content in street dust as a reflection of atmospheric dust emissions from coal power plants, metal smelters, and traffic. Environ. Sci. Pollut. R. 20 (7), 4455–4468.